



OPEN

# Black electrochromic ink with a straightforward method using copper oxide nanoparticle suspension

Chan Yang Jeong, Hiroshi Watanabe &amp; Kazuki Tajima

Electrochromic (EC) materials for smart windows must exhibit a dark colour and block visible light (wavelength = 380–780 nm) to reduce environmental impact. In particular, black tones are also desired, and there are many reports of attempts to create these dark tones using organic materials such as polymers. However, their fabrication methods are complicated, expensive, and may even use hazardous substances; moreover, they are often not sufficiently durable, such as upon exposure to ultraviolet light. There are some reported cases of black materials using the CuO system as an inorganic material, but the synthesis method was complicated and the functionality was not stable. We have found a method to synthesize CuO nanoparticles by simply heating basic copper carbonate and adjusting the pH with citric acid to easily obtain a suspension. The formation and functionality of CuO thin films were also demonstrated using the developed suspension. This research will enable the creation of EC smart windows using existing inorganic materials and methods, such as printing technology, and is the first step towards developing environment-friendly, cost-effective, and functional dark inorganic materials.

Electrochromic (EC) materials exhibit reversible optical properties via electrochemical redox reactions, making it possible to control the transmittance and absorption in the near-infrared (NIR) and visible regions<sup>1,2</sup>. Owing to this unique ability, EC materials can be exploited to develop electrochromic devices (ECDs), which are widely used for displays<sup>3</sup>, sensors<sup>4</sup>, energy storage devices<sup>5</sup>, and smart windows<sup>6,7</sup>. The EC materials are mainly categorised as inorganic or organic. Inorganic materials include transition metal oxides (e.g., tungsten oxide<sup>8</sup>, nickel oxide<sup>9</sup>) and inorganic complexes (e.g., organic framework<sup>10</sup>). Organic materials consist of  $\pi$ -conjugated organic molecules (e.g., viologen<sup>11</sup>), conductive polymers (e.g., polyimide<sup>12</sup>, polythiophene<sup>13</sup>), etc. Inorganic EC materials offer several advantages over organic ones, including high chemical stability and efficiency, as well as a memory effect after removing the external voltage, which are significant factors governing ECD applications<sup>1</sup>.

Among the existing EC materials in ECDs, those that switch between transparent and blue-tinted states have already been commercialised<sup>14</sup>, but grey or black tints are now required to meet the recent demand for darker states for both design reasons and to reduce environmental impact. If such material systems can be realised, they can be used as a window material in next-generation vehicles, such as electric vehicles and fuel cell vehicles, which are expected to become more popular in the future. When applied in windows, these materials can decrease electricity costs and increase the cruising range of these vehicles by reducing the air conditioning load.

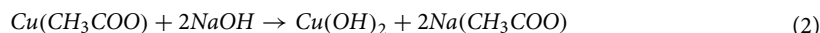
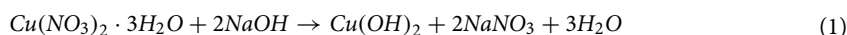
To date, several studies have demonstrated black EC materials. However, many of these reported materials remain in the basic research stage because they are organic<sup>15–18</sup>, require a variety of materials for synthesis, are complex and time-consuming to process, and in some cases have a large environmental impact. Therefore, EC material systems that can express black in a simpler way are required.

Our group has been developing inks based on aqueous dispersions of tungsten oxide (WO<sub>3</sub>) and PB nanoparticles (NPs) for application in wet processes to prepare EC thin films<sup>8,10</sup>. Among wet processes, printing<sup>19</sup> and coating<sup>20,21</sup> offer the advantage of enabling EC thin film fabrication on large-scale substrates in a short time and at a low cost. In addition, these techniques are advantageous for thin film preparation on glass substrates and flexible substrates.

In this study, we developed a simple method for preparing dispersed suspensions of CuO NPs using basic copper(II) carbonate as the starting material and citric acid to adjust the pH of the water. Although methods for

National Institute of Advanced Industrial Science and Technology (AIST), 1-1-1 Higashi, Tsukuba, Ibaraki 305-8565, Japan. email: k-tajima@aist.go.jp

producing nanosized CuO particles have been extensively investigated<sup>22–25</sup>, there has been very little research on the preparation of stable, dispersed CuO NP suspensions, which are essential liquid-phase coatings for thin film production<sup>26,27</sup>. Biomedical applications of CuO NPs, for example, as sensor materials, glucose sensors, H<sub>2</sub>O<sub>2</sub> sensors, dopamine sensors, and wound healing are well reported<sup>28</sup>. Colloidal suspensions containing oxide NPs have significant potential for application on an industrial scale, because they are easy to apply in continuous production processes, such as the printing and coating of nanostructured films<sup>29</sup>. Several attempts have been made to prepare CuO colloidal suspensions using nitrate- and acetate-based solutions<sup>26,30–32</sup>.



However, these processes are toxic to humans and require careful handling. They are also difficult to implement commercially when complex synthesis methods are required. Thus, the effective and cost-effective production of enough products within a given period to make these processes economically viable is a significant challenge.

In contrast to these previously reported methods, our process used no other materials like sodium hydroxide. In general, pure CuO particles do not disperse in water. Therefore, the surface of CuO was modified by adding citric acid to improve the water dispersibility (Fig. 1a). The NPs and dispersions of iron oxide, silver, and copper oxide have been prepared using citric acid in several studies, but they used materials that require careful handling, such as NaOH and metal nitrite<sup>33–35</sup>. There has been no report of the successful preparation and dispersion of such particles using citric acid alone thus far. In addition, CuO thin films are typically prepared by several different conventional methods, such as electrodeposition<sup>36</sup>, sol-gel<sup>12</sup>, and sputtering<sup>37</sup>. However, these methods are time-consuming and cannot be used to easily manufacture a large film. Therefore, some researchers have attempted to prepare large thin films in a short time at a low cost by coating or printing dispersed NP suspensions. In this study, we evaluated the applicability of a dispersed CuO NP suspension for coating functional thin films.

Furthermore, although CuO thin films offer many applications, such as batteries, gas sensors, and solar cells, this study was focused on their EC behaviour, which is a functional property of CuO. Richardson et al.<sup>38</sup> observed that CuO thin films prepared by sputtering appeared dark in the coloured state. Therefore, the development of

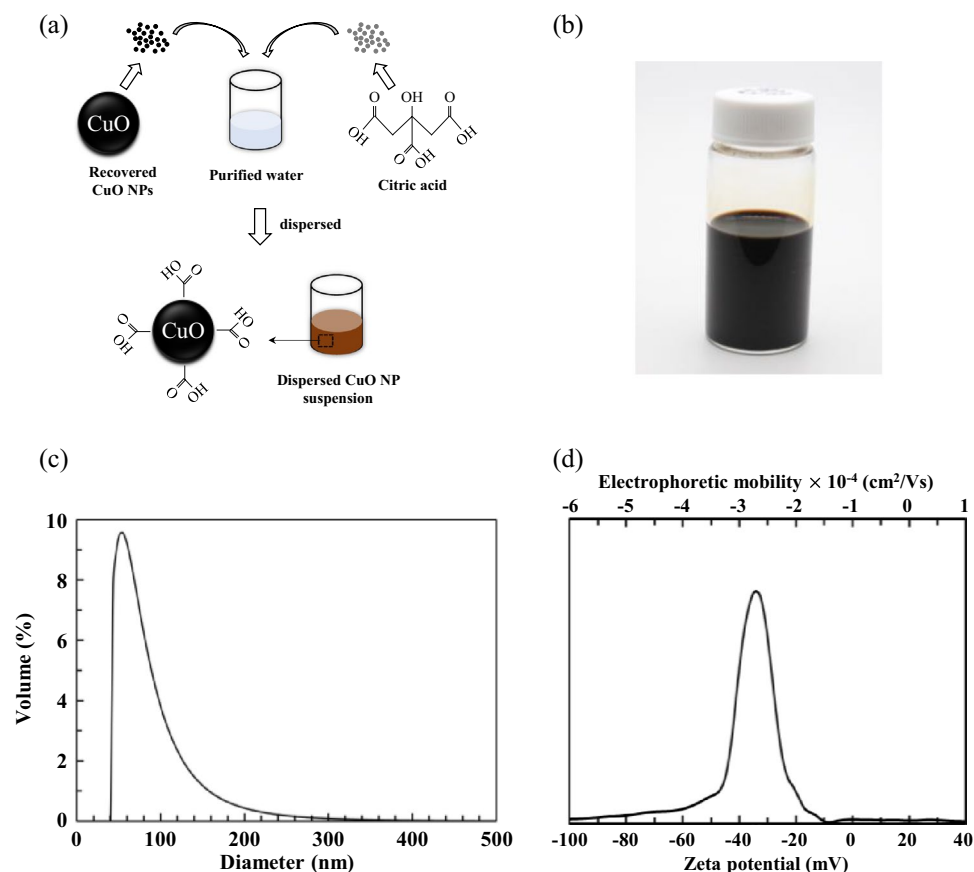


**Figure 1.** (a) Schematic of dispersed CuO NP suspension preparation and (b) photograph of prepared CuO suspension. (c) Mean (volume) diameter of the prepared CuO NP dispersed suspensions. (d) Zeta potential of the CuO suspensions.

a coating method that can be used to easily fabricate large-size CuO has tremendous potential to replace conventional black organic EC materials<sup>16,39–42</sup>.

To that end, we used a dispersed CuO NP suspension to coat a functional thin film on an indium tin oxide (ITO)-coated glass substrate. Additionally, polyvinyl alcohol (PVA) was used to improve the adhesion of the CuO NPs to the ITO substrate in the thin films. The prepared CuO thin film exhibited a large change in the transmittance of 70%  $\leftrightarrow$  6% at a wavelength of 633 nm via an electrochemical redox reaction, suggesting the possibility of producing a black material as an inorganic material. When understanding electrochemical behaviour and EC properties as one of the functionalities of CuO thin film, the treatment of the reaction mechanism and other aspects of the electrochemical behaviour is complicated due to the existence of various electrolytes and other cell structures. In order to use CuO as a stable black electrochromic material, it was assumed that it would be difficult to analyze the detailed reaction mechanism in thin films prepared by existing methods. However, the synthesis method of CuO-based nanoparticle suspensions discovered in this study enabled us to proceed with a detailed mechanism analysis of the electrochromic properties of the resulting CuO thin films.

## Results

**Formation of dispersed CuO NP suspension.** The surface tension and viscosity of the dispersed CuO NP suspension synthesized by the procedure in Fig. 1a were 69 mN/m and 1.19 cP, respectively. A photograph of the suspension is shown in Fig. 1b. The density and pH of the suspension were 4.67 g/cm<sup>3</sup> and 6.0, respectively.

The volume mean diameter of the particles in the synthesised CuO NP suspensions was determined to be 56 nm using dynamic light scattering (DLS) measurements (Fig. 1c). In addition, the zeta potential was measured to analyse the stability of the CuO suspension, which indicates the possible behaviour of the dispersion. The CuO suspensions under three different PVA conditions are shown in Fig. 1d. A mean zeta potential of  $-34.9$  mV was obtained for the suspensions; zeta potential values between  $-30$  and  $-40$  mV typically indicate moderate stability<sup>43,44</sup>. For comparison, colloidal solutions were prepared with 95.0% and 99.9% copper(II) oxide, which are commercially available, under the same conditions used to synthesise the CuO NPs. However, these powders did not disperse well in water containing dissolved citric acid (Supplementary Fig. S1).

**Structure and chemical composition of the CuO nanoparticles and films.** To determine the crystal structure and phase composition of the CuO NPs obtained after solvent evaporation at 120 °C in a dry oven and the CuO film prepared by the spin-coating method (Fig. 2a), X-ray diffraction (XRD) patterns were recorded for all synthesised samples, as shown in Fig. 2b. The XRD patterns of the CuO nanopowders were identical to that of monoclinic single-phase CuO, and the diffraction data corresponded well with that of the CuO JCPDS card (JCPDS 45-0937), with no impurity peaks present. Furthermore, the primary crystallite size ( $\sim 20$  nm) determined by the Pawley method, combined with the results of XRD analysis, confirmed the material dispersed in the suspension to be CuO NPs. Interestingly, a (220) peak, corresponding to Cu<sub>2</sub>O (JCPDS

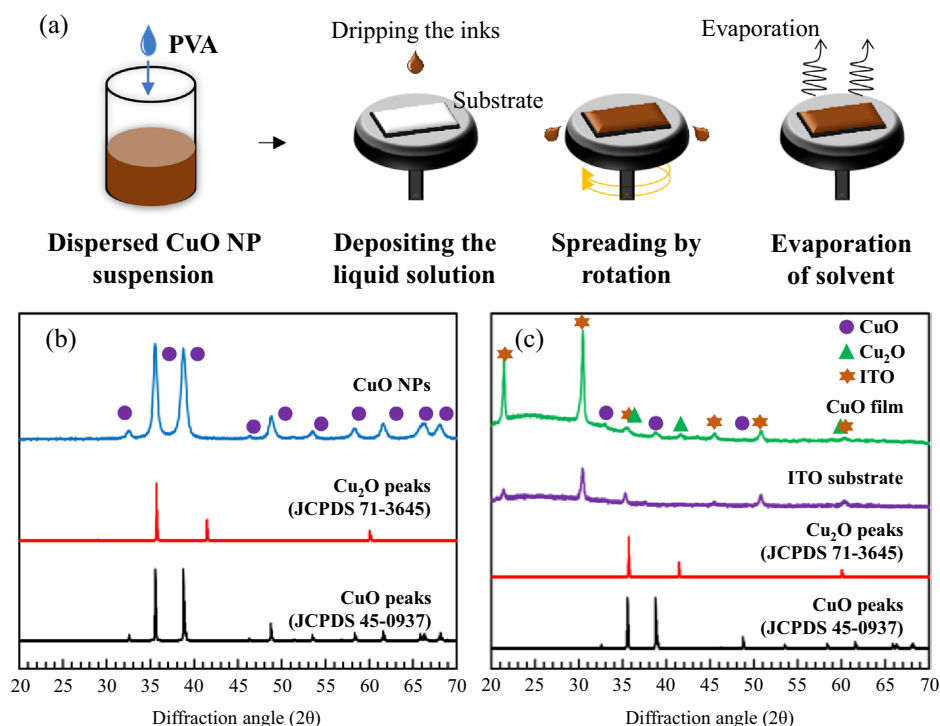


**Figure 2.** (a) Schematic of CuO film preparation. (b) XRD patterns of nanopowders obtained from solvent-evaporated dispersed CuO NP suspensions and (c) CuO thin films coated on ITO substrates.

71-3645), was observed at  $\sim 42^\circ$  for the spin-coated films, as shown in Fig. 2c. This peak may indicate that  $\text{Cu}_2\text{O}$  is formed in the outer layers of the film owing to the partial reduction of  $\text{Cu(II)}$  to  $\text{Cu(I)}$ .

X-ray photoelectron spectroscopy (XPS) was employed to investigate the chemical composition of the  $\text{CuO}$  NP powders and  $\text{CuO}$  films prepared on the ITO substrates (Supplementary Table S1). The XPS survey spectra of the  $\text{CuO}$  films showed no impurity peaks, and exhibited only the peaks corresponding to  $\text{Cu}$ ,  $\text{O}$ , and  $\text{C}$ . Figures 3a-1, b-1 show the high-resolution spectra of  $\text{Cu } 2p$ , which are separated into the  $\text{Cu } 2p_{3/2}$  and  $\text{Cu } 2p_{1/2}$  peaks observed at approximately  $932.3 \pm 0.1$  eV and  $952.2 \pm 0.3$  eV, respectively<sup>45,46</sup>. The distance between these  $\text{Cu } 2p$  main peaks was 19.9 eV, which agreed with that reported for the  $\text{CuO}$  spectrum<sup>47</sup>. Moreover, Fig. 3a-1, b-1 clearly show that the  $\text{Cu } 2p$  spectra contain “shake-up” satellites, which are characteristic of the  $\text{Cu}^{2+}$  state<sup>45</sup>. These satellite peaks are deviated by  $\sim 9$  eV from the main peak (the binding energies ( $E_b$ ) are approximately 941 and 962 eV for  $\text{Cu } 2p_{3/2}$  and  $\text{Cu } 2p_{1/2}$ , respectively). Intense peaks corresponding to  $\text{Cu}^{2+} 2p_{3/2}$  and  $\text{Cu}^{2+} 2p_{1/2}$  were observed for the  $\text{CuO}$  NPs, indicating that the prepared NP sample contained  $\text{CuO}$  (Fig. 3a-1). In contrast, intense  $\text{Cu}^+ 2p_{3/2}$  and  $\text{Cu}^+ 2p_{1/2}$  peaks were observed for the  $\text{CuO}$  film prepared on the ITO substrate. This indicates that the film primarily contains  $\text{CuO}$ , and the outer layer contains  $\text{Cu}_2\text{O}$ , in which  $\text{Cu(II)}$  partially oxidised to  $\text{Cu(I)}$ <sup>48</sup>. This was in agreement with the XRD results. The  $\text{O } 1s$  XPS profiles are presented in Fig. 3a-2, b-2. A clear peak is observed at  $530.3 \pm 0.2$  eV, which can be indexed to  $\text{O}^{2-}$  in  $\text{CuO}$ <sup>49</sup>. Notably, three other weak  $\text{O } 1s$  peaks are also present. The peak located at  $531.7 \pm 0.2$  eV originates due to surface hydroxyls<sup>49,50</sup>, while the peaks at 532.5 and 533.8 eV correspond to  $\text{C}=\text{O}$  and  $\text{C}-\text{O}$ , respectively<sup>51</sup>. The latter peaks can be attributed to the citric acid and PVA used in the preparation of the dispersed  $\text{CuO}$  NP suspension. The  $\text{C } 1s$  signal of the  $\text{CuO}$  films (284.8 eV) in Fig. 3a-3, b-3 can be attributed to the  $\text{C}-\text{C}$  bonds of PVA and citric acid<sup>48,52</sup>.

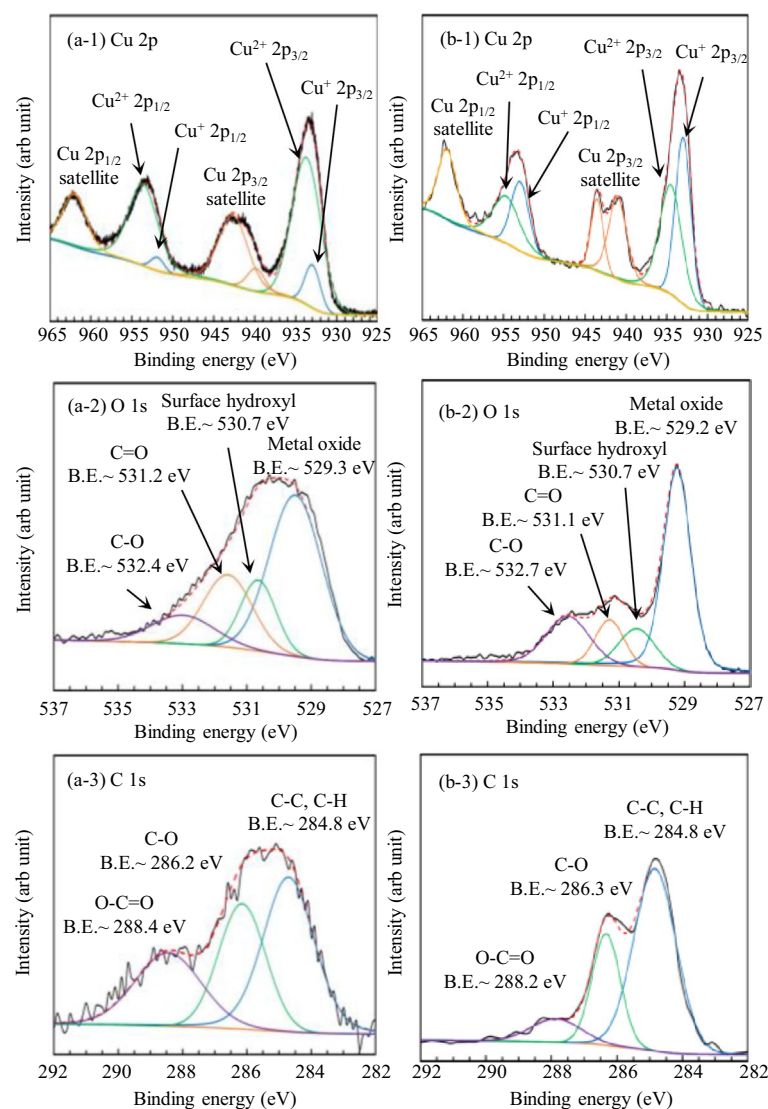


**Figure 3.** High-resolution XPS profiles of (a) nanopowders obtained from solvent-evaporated dispersed  $\text{CuO}$  NP suspensions and (b)  $\text{CuO}$  thin films prepared on ITO substrates.

To investigate the effect of PVA addition on the film-forming characteristics of CuO NP suspensions, field-emission scanning electron microscopy (FESEM) was used to study their morphological features. Supplementary Fig. S2 shows the surface and cross-sectional FESEM images of 1 wt.% PVA CuO films. From the cross-sectional image shown in Supplementary Fig. S2a, the CuO films are approximately 200 nm thick and exhibit good adhesion between the ITO substrates and CuO coatings. Furthermore, the surface morphology seen in Supplementary Fig. S2b indicates that the film exhibits a porous structure. This porous structure could enhance the  $\text{Li}^+$  diffusion in the film and contribute to its cationic conductivity<sup>53</sup>.

**Electrochemical and electrochromic properties.** The electrochemical and EC properties of the CuO films deposited on the ITO substrates were analysed using a three-electrode chemical cell containing aqueous  $\text{LiClO}_4/\text{PC}$  (1 mol/kg) as the electrolyte. The cyclic voltammetry (CV) measurements were conducted in the potential range from  $-1.8$  to  $+1.3$  V vs. Ag/AgCl at a sweep rate of 5 mV/s. The results are shown in Fig. 4a and Supplementary Fig. S3. The CuO film exhibits a complex redox reaction, and we propose the following four steps of electrochemical reaction mechanism. (1) The prepared thin film is in a state in which CuO and  $\text{Cu}_2\text{O}$  are a mixture at the beginning of the reaction. (2) A cathodic peak<sup>54</sup>, which corresponds to  $\text{Cu}_2\text{O} + 2\text{CuO} + 2\text{Li}^+ + 2\text{e}^- \rightarrow 2\text{Cu}_2\text{O} + \text{Li}_2\text{O}$ <sup>55-57</sup>, appeared at approximately  $-0.5$  V, and the transmittance increased slightly to  $-1.2$  V. This is attributed to the reduction of CuO present in the thin film to  $\text{Cu}_2\text{O}$ , and is consistent with the XPS results described above. (3) Furthermore, an oxidation reaction, which corresponding to  $2\text{Cu}_2\text{O} + 2\text{Li}_2\text{O} \rightarrow 4\text{CuO} + 4\text{Li}^+ + 4\text{e}^-$ <sup>56</sup>, was initiated at approximately  $-1.8$  V, which caused the film colour to change to dark. A peak corresponding to CuO was observed in the XPS results of the black CuO thin film (Supplementary Fig. S4), and it is considered that  $\text{Cu}_2\text{O}$ <sup>58</sup> and  $\text{Li}_2\text{O}$ <sup>59</sup> did not fully participate. Finally, (4) it is thought that the film becomes CuO state due to  $4\text{CuO} + 2\text{Li}^+ + 2\text{e}^- \rightarrow 2\text{CuO} + \text{Cu}_2\text{O} + \text{Li}_2\text{O}$  at approximately  $-0.2$  V. The transferred charge density ( $\Delta Q$ ), which indicates the electrochemical activity of the CuO film, was determined by performing chronocoulometry (CC) at constant applied potentials of  $-1.8$  and  $+1.3$  V (vs. Ag/AgCl) for 90,

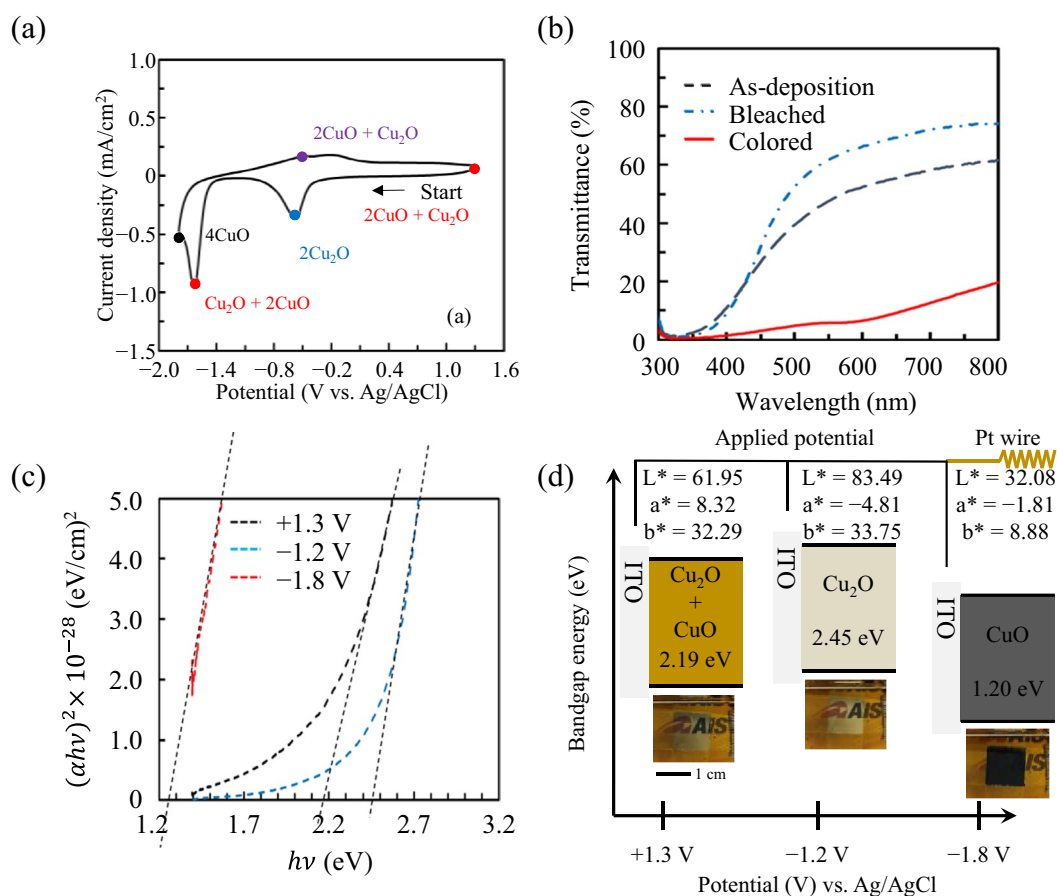


**Figure 4.** Electrochemical and EC properties of the CuO films in  $\text{LiClO}_4/\text{PC}$  (1 mol/kg) electrolyte solution. **(a)** CV profiles of CuO thin films. The potential scan rate was 5 mV/s. **(b)** Bleached (blue line), coloured (red line), and as-prepared (black line) transmittance spectra of CuO thin films. Constant voltages of  $-1.8$  and  $+1.3$  V (vs. Ag/AgCl) were applied for 30 s each to colour and bleach the films, respectively. **(c)**  $(\alpha hv)^2$  vs. photon energy for CuO thin films in as-prepared, coloured at  $-1.8$  V and bleached at  $+1.3$  V states. Intercepts of the dashed lines correspond to the direct band gaps. **(d)** Schematic representation of the energy band diagram and photos of the CuO composite.

120, and 120 s, respectively, to allow sufficient time for the complete redox reaction in each film (Supplementary Fig. S5). A  $\Delta Q$  value of 68 mC/cm<sup>2</sup> was observed for the CuO film.

Changes in the optical transmittance spectra of the as-deposited, transparent brown, and dark grey colour states of the CuO films were studied using ultraviolet–visible (UV–Vis) spectroscopy during CC analysis, as shown in Fig. 4b. The change in the transmittance of the CuO film with a thickness of 200 nm at +1.3 and –1.8 V was approximately 63% at a wavelength of 633 nm. However, the transmittance of the 150-nm-thick film in the coloured state increased, and the transmittance of the 300-nm-thick film in the bleached state decreased (Supplementary Fig. S6). Therefore, the film thickness of 200 nm was considered the most appropriate for application as an EC material. Moreover, the optical density ( $\Delta OD$ ) was used to calculate the EC colouration efficiency (CE), which is an important EC parameter that determines the electrochemical performance of the films (Supplementary Table S2). This parameter is defined in Eqs. (3) and (4):

$$CE = \frac{\Delta OD}{\Delta Q} \quad (3)$$

$$\Delta OD(\lambda) = \log_{10}(T_{\lambda b}/T_{\lambda c}) \quad (4)$$

where  $\lambda = 633$  nm, and  $T_{\lambda b}$  and  $T_{\lambda c}$  represent the transmittance of the bleached and coloured states, respectively. The  $\Delta OD$  and CE values obtained for the CuO films were 1.04 and 15.36 cm<sup>2</sup>/C, respectively.

The band gaps ( $E_g$ ) of the films in the as-deposited, transparent brown, and dark grey states can be estimated using the transmittance data and estimated film thickness ( $d = 200$  nm). Figure 4c shows a graphical representation of  $(\alpha hv)^2$  vs. photon energy ( $hv$ ) for these states, which can be evaluated using the following equation<sup>54,60,61</sup>:

$$\alpha = \frac{1}{d} \ln \frac{100}{T} \quad (5)$$

where  $\alpha$ ,  $d$ , and  $T$  are the absorption coefficient, film thickness, and transmittance value, respectively. The optical density can be used to obtain the band gap energy of the transparent films by plotting  $(\alpha hv)^{1/\eta}$  against  $hv$ , based on the following relation<sup>58–61</sup>:

$$\alpha hv = A(hv - E_g)^\eta \quad (6)$$

where  $A$  and  $\eta$  are constants, and  $\eta$  depends on the nature of the transition. For copper-oxide-based materials, it is assumed that  $\eta = 1/2$ , which corresponds to a directly allowed electron transition mechanism<sup>48,50,52</sup>. Therefore, in the initial absorption region ( $hv \approx E_g$ ), where the plot of  $(\alpha hv)^2$  vs.  $hv$  is linear, the intercept of the extrapolated fitted line with the  $hv$  axis gives the optical band gap energy, as shown in Fig. 4c. Direct optical band gap energies for the Cu<sub>2</sub>O and CuO films, which have been reported to be in relatively wide ranges of approximately 2.1–2.6 eV and 1.3–1.7 eV, respectively<sup>54,62–67</sup> are dependent on the fabrication method and stoichiometry. The experimentally obtained optical band gap values were compared with the reported data, as shown in Fig. 4d. The transmittance in the as-deposited state, the transparent brown state, and the dark grey state corresponded to the Cu<sub>2</sub>O + CuO compound film, Cu<sub>2</sub>O, and CuO + Cu films, respectively. The colour details were also evaluated based on the band gap change using the International Commission on Illumination (CIE: usually abbreviated CIE for its French name, Commission Internationale de l’Eclairage) 1976 L\*a\*b\* colour model. The L\* and b\* values decreased from 83 to 32 and from 34 to 9, respectively, and the a\* value increased from –5 to –2 as Cu<sub>2</sub>O was oxidised to CuO, which is indicative of a nearly dark grey colour (Supplementary Fig. S7). Several groups previously reported the chromaticity of dark organic EC materials prepared by different techniques. For instance, Wu et al.<sup>68</sup> observed that the L\* values of amine-based organic EC materials decreased from 92 to 6 upon changing from the bleached to the coloured state. Further, Liu et al.<sup>42</sup> also reported a change in L\* between 88 and 7 with an organic EC device composed of polyamide and viologen.

Here, we summarise the superiority of the results of this study by comparing them with those of existing studies. Although organic materials exhibit excellent EC properties, they have several disadvantages, including the use of harmful substances and complicated manufacturing processes, as well as poor durability against external stimuli (UV, temperature, etc.). In contrast, the CuO ink used in this study can be synthesised simply by mixing basic copper(II) carbonate with citric acid, which enabled coating CuO thin films. Furthermore, the CuO thin film prepared in this study showed better EC properties than any previously reported CuO thin films in Li-based electrolytes<sup>54</sup> and showed low transmittance at visible wavelengths of 380–780 nm, which is comparable to that of organic EC materials. Moreover, as a nanomaterial, the CuO ink in this study has many potential applications at the cutting edge of science and technology, including catalysis<sup>69</sup>, gas sensors<sup>70</sup>, photovoltaic cells<sup>71</sup>, light-emitting diodes<sup>72</sup>, magnetic phase transitions<sup>73</sup>, and superconductors<sup>74</sup>.

## Discussion

We developed a facile method for synthesising dispersed CuO NP suspensions using only citric acid, basic copper(II) carbonate, and water. This method does not require conventional toxic chemicals such as metal nitrite or NaOH and significantly reduces the suspension preparation time and cost. The PVA was added to the suspensions to help evaluate the ability to deposit CuO thin films on an ITO substrate by spin coating, which is an inexpensive and simple film preparation method. The XRD results indicated strong CuO peaks for the powder obtained from the suspensions; however, Cu<sub>2</sub>O (200) peaks appeared for the spin-coated films. This may indicate the formation of Cu(II) in the outer layers of the film owing to the partial oxidation of Cu(I), which is consistent with the XPS results. The CV profiles displayed redox peaks, which corresponded to the reversible transition between Cu<sub>2</sub>O and CuO. The films also exhibited EC behaviour during the redox reaction; the colour changed

to grey and transparent brown at negative and positive voltages, respectively. The difference in transmittance values between the grey and transparent film states at 633 nm was ~40%. The band gaps for the three film states (as-prepared, dark grey, and transparent brown) were determined from the transmittance measurements, based on a direct semiconductor transition mechanism. These results confirmed that the EC process was driven by the conversion of  $\text{Cu}_2\text{O}$  to  $\text{CuO}$  in a reversible redox reaction on the film surface. Because this material is suggested to be superior to organic black EC materials in terms of lightfastness (life span), environmental testing is scheduled to demonstrate its practical feasibility. In particular, in an ongoing research project (JST A-STEP (Grant Number JPMJTR203D)), we are conducting research and development of black EC devices that can be mounted on automobile window glass in collaboration with a company. Although there are many materials and principles of blue and transparent colour change in commercial EC devices, since blue tones have compatibility and affinity with body colours when installed in automobiles, "blackness" is one of the important development elements not only in terms of mere functionality, but also in terms of design. Furthermore, in Japan, for example, there is a large temperature difference between the four seasons ( $-20^\circ\text{C}$  in winter and nearly  $40^\circ\text{C}$  in summer), and the rainy season is a very harsh natural environment. Therefore, based on the results obtained in this study, the company plans to convert to a stable deposition process (large area and uniformity) and advance the durability (light resistance, heat and humidity resistance, etc.) required for in-vehicle applications. The results obtained in terms of durability and other aspects, as well as approaches to overcoming issues, will be reported continuously in the future. Finally, although the main research objective of this study was to create black EC materials, the  $\text{CuO}$  NP dispersion suspensions produced by this extremely simple method could be applied in dye-sensitised solar cells, gas sensors, batteries, and EC devices using other coating technologies such as inkjet and slit coating.

## Methods

**Reagents.** The following reagents were purchased and used without further purification: basic copper(II) carbonate ( $\text{Cu}_2\text{CO}_3(\text{OH})_2$ ; FUJIFILM Wako Pure Chemical Co.), citric acid ( $\text{C}_6\text{H}_8\text{O}_7$ ; FUJIFILM Wako Pure Chemical Co.), polyvinyl alcohol (PVA; 99%; Japan Vam & Poval Co., Ltd.), and lithium perchlorate ( $\text{LiClO}_4$ ; FUJIFILM Wako Pure Chemical Co.). The ITO-coated glass with a surface resistivity of  $10\ \Omega/\text{sq}$  was obtained from Geomatec.

**Synthesis of dispersed  $\text{CuO}$  nanoparticle suspension.** The  $\text{CuO}$  NPs were obtained by thermally treating basic copper carbonate at  $320^\circ\text{C}$  for 3 h using a muffle furnace (FP21, Yamato Scientific Co.) under atmospheric conditions<sup>75</sup>. A citric acid solution (2.0 M, pH: 3.0) was prepared using purified water before adding the  $\text{CuO}$  NPs. The pH of the citric acid solution was ~2.5. Next, the  $\text{CuO}$  NPs (20% of the total ink weight) were mixed in purified water by stirring for 24 h at 1000 rpm at room temperature ( $\sim 20^\circ\text{C}$ ). The  $\text{CuO}$  NPs were then recovered by centrifugal separation at 18,000g for 10 min. Subsequently, the  $\text{CuO}$  NPs were dispersed by adding pure water to prepare a  $\text{CuO}$  NP suspension. Regarding these synthesis methods, our research group has expertise in the synthesis of Prussian blue NP and follows that method<sup>76,77</sup>. The  $\text{CuO}$  content in the final suspension was maintained at 20% of the total weight. The process for synthesising the dispersed  $\text{CuO}$  NP suspensions is shown in Supplementary Fig. S8.

**Particle size and zeta potential.** Since the synthesized  $\text{CuO}$  NP were expected to be quite small in this study, the volume-averaged diameter and zeta potential of the dispersed  $\text{CuO}$  NP suspension were measured by Dynamic Light Scattering (ELS-Z 2, Otsuka Electronics Co., Ltd.).

**Film preparation.** The viscosity of the as-prepared suspension was low, making it difficult to prepare the  $\text{CuO}$  thin films. Thus, to improve the adhesion of the  $\text{CuO}$  NP suspension to the ITO glass substrate and increase its viscosity, 1 wt.% PVA was added. Prior to film preparation, a  $25\text{-cm}^2$  ITO substrate was subjected to plasma treatment for 3 min using a plasma cleaner (PDC-001, Harrick Plasma Inc.) to increase its wettability towards the  $\text{CuO}$  suspension. Plasma processing was performed under a radio frequency (RF) glow discharge at a low pressure of  $1 \times 10^{-3}$  Torr and an applied wattage of 30 W. The  $\text{CuO}$  thin films were then deposited on the ITO substrates using a spin-coating machine (ACT-300AII, Active Inc.). To evaluate the characteristics of the film,  $\text{CuO}$  thin film samples (sizes:  $2.5\ \text{cm}^2$  for XRD and  $1\ \text{cm}^2$  for XPS/FESEM) were prepared after cutting them with a diamond blade.

**Film characterisation.** The crystallinity of the  $\text{CuO}$  nanopowders was determined by first evaporating the solvent from the NP suspension at  $120^\circ\text{C}$  in a dry oven. The powders were then analysed by XRD at 40 kV and 40 mA using Cu-K $\alpha$  radiation ( $\lambda = 1.5418\ \text{\AA}$ ) (D8 Advance, Bruker AXS Inc.); the data were collected within a diffraction angle ( $2\theta$ ) range of  $20^\circ$ – $80^\circ$ . The size of the primary crystallites was calculated with TOPAS V5.0 software using the Pawley method. The XPS (PHI 5000 Versaprobe; Ulvac-Phi, Inc.) was conducted with Al-K $\alpha$  radiation. Survey scans were recorded in the range of 0–1000 eV, with a pass energy of 117.4 eV and resolution of 0.2 eV. High-resolution scans were obtained at a pass energy and resolution of 23.5 and 0.025 eV, respectively. To avoid sample charging, a neutraliser filament was used. Adventitious carbon, with a C 1s peak at 284.8 eV, was used to calibrate the spectra and correct for peak shifts due to charging. The obtained Cu 2p XPS profiles were deconvoluted using a nonlinear least-squares curve-fitting program (MultiPak Version 9.6 software), and the Shirley background was used for spectral deconvolution. The peaks were mixed (80% Gaussian and 20% Lorentzian) and constrained by a Cu  $2p_{3/2}$ –Cu  $2p_{1/2}$  spin-orbit separation of 19.9 eV; the area ratio of the two peaks in each doublet was 0.75. Qualitative XPS scans of the  $\text{CuO}$  films were generated in the binding energy ( $E_b$ ) range of 925–970 eV. The cross-sectional morphologies of the films and their thicknesses were characterised by

FESEM (S-4800; Hitachi, Ltd., Japan) with an accelerating voltage of 5 kV after coating the samples with Pt–Pd using an ion sputter coater (E-1030; Hitachi, Ltd., Japan).

The deposition density of the CuO suspension was calculated using Eq. (7)<sup>78</sup>:

$$\rho = m/(A \times d) \quad (7)$$

where  $d$  is the film thickness,  $m$  is the weight of the coated dispersed CuO NP suspension,  $A$  is the area of the ITO substrate, and  $\rho$  is the suspension density. The  $d$  values of the CuO films were estimated by FESEM through the cross-sectional morphology of the films. A thickness of 200 nm was observed for the prepared CuO film, and the calculated  $\rho$  was 4.67 g/cm<sup>3</sup>.

**Electrochemical and electrochromic analysis.** To investigate the electrochemical and EC properties of the films, CV and CC measurements were performed using aqueous LiClO<sub>4</sub>/PC (1.0 mol/kg), which is a polymer that contains a Li salt, in a conventional three-electrode cell with an electrochemical measurement system (6115D, ALS/HCH). A WO<sub>3</sub> film deposited on the ITO substrate served as the working electrode; a Pt wire was used as the counter electrode, and Ag/AgCl was used as the reference electrode; LiClO<sub>4</sub> was used as a supporting electrolyte. The in-situ transmittance was determined using a multichannel charge-coupled device (CCD) detector (DH-2000, Ocean Optics). The chromaticity of the 200-nm CuO film was measured using a spectrophotometer (SD 3000, Nippon Denshoku Industries Co. Ltd.).

### Data availability

The data supporting the findings of this study are available from the corresponding author upon reasonable request.

Received: 21 February 2023; Accepted: 9 May 2023

Published online: 13 May 2023

### References

- Mortimer, R. J. Electrochromic materials. *Annu. Rev. Mater. Res.* **41**, 241–268 (2011).
- Rougier, A., Sauvet, K. & Sauques, L. Electrochromic materials from the visible to the infrared region: An example WO<sub>3</sub>. *Ionic* **14**, 99–105 (2008).
- Cho, S. I. *et al.* Nanotube-based ultrafast electrochromic display. *Adv. Mater.* **17**, 171–175 (2005).
- Xu, W., Fu, K. & Bohn, P. W. Electrochromic sensor for multiplex detection of metabolites enabled by closed bipolar electrode coupling. *ACS Sens.* **2**, 1020–1026 (2017).
- Yang, P., Sun, P. & Mai, W. Electrochromic energy storage devices. *Mater. Today* **19**, 394–402 (2016).
- Xie, Z. *et al.* Integrated smart electrochromic windows for energy saving and storage applications. *Chem. Commun.* **50**, 608–610 (2014).
- Piccolo, A. & Simone, F. Performance requirements for electrochromic smart window. *J. Build. Eng.* **3**, 94–103 (2015).
- Jeong, C. Y., Watanabe, H. & Tajima, K. Flexible electrochromic devices based on tungsten oxide and Prussian blue nanoparticles for automobile applications. *Electrochim. Acta* **11**, 28614–28620 (2021).
- Chen, P.-W. *et al.* Fast response of complementary electrochromic device based on WO<sub>3</sub>/NiO electrodes. *Sci. Rep.* **10**, 8430 (2020).
- Yu, F. *et al.* Electrochromic two-dimensional covalent organic framework with a reversible dark-to-transparent switch. *Nat. Commun.* **11**, 5534 (2020).
- Madasamy, K., Velayutham, D., Suryanarayanan, V., Kathiresan, M. & Ho, K.-C. Viologen-based electrochromic materials and devices. *J. Mater. Chem. C* **7**, 4622–4637 (2019).
- Wang, H.-M. & Hsiao, S.-H. Ambipolar, multi-electrochromic polypyromellitimides and polynaphthalimides containing di(*tert*-butyl)-substituted bis(triarylamine) units. *J. Mater. Chem. C* **2**, 1553–1564 (2014).
- Welsh, T. A. & Draper, E. R. Water soluble organic electrochromic materials. *RSC Adv.* **11**, 5245–5264 (2021).
- Moretti, C., Tao, X., Koehl, L. & Koncar, V. Electrochromic textile displays for personal communication, in *Smart Textiles and Their Applications* (Koncar, V. Ed.). 539–568 (Woodhead Publishing, 2016).
- Xu, Z. *et al.* Colour tuning for black-to-transmissive conjugated copolymer with excellent electrochromic properties via electrochemical copolymerization of two donor-acceptor type monomers. *Mater. Des.* **194**, 108903 (2020).
- Li, M. *et al.* Colourless to black electrochromic devices using subtractive colour mixing of two electrochromes: A conjugated polymer with a small organic molecule. *Org. Electron.* **84**, 105748 (2020).
- Zeng, J. *et al.* Colourless-to-black electrochromic materials and solid-state devices with high optical contrast based on cross-linked poly(4-vinyltriphenylamine). *Sol. Energy Mater. Sol. Cells* **195**, 89–98 (2019).
- Yu, X. *et al.* Colourless-to-black electrochromism from binary electrochromes towards multifunctional displays. *ACS Appl. Mater. Interfaces* **12**, 39505–39514 (2020).
- Cai, G. *et al.* Inkjet-printed all solid-state electrochromic devices based on NiO/WO<sub>3</sub> nanoparticle complementary electrodes. *Nanoscale* **8**, 348–357 (2016).
- Li, X., Perera, K., He, J., Gumyusenge, A. & Mei, J. Solution-processable electrochromic materials and devices: Roadblocks and strategies towards large-scale applications. *J. Mater. Chem. C* **7**, 12761–12789 (2019).
- Tajima, K. *et al.* Green fabrication of a complementary electrochromic device using water-based ink containing nanoparticles of WO<sub>3</sub> and Prussian blue. *RSC Adv.* **10**, 2562 (2020).
- Ko, S., Lee, J. I., Yang, H. S., Park, S. & Jeong, U. Mesoporous CuO particles threaded with CNTs for high-performance lithium-ion battery anodes. *Adv. Mater.* **24**, 4451–4456 (2012).
- Li, Y., Liang, J., Tao, Z. & Chen, J. CuO particles and plates: Synthesis and gas-sensor application. *Mater. Res. Bull.* **43**, 2380–2385 (2008).
- Filipić, G. & Cvelbar, U. Copper oxide nanowires: A review of growth. *Nanotechnology* **23**, 194001 (2012).
- Li, Y., Yang, X. Y., Feng, Y., Yuan, Z. Y. & Su, B. L. One-dimensional metal oxide nanotubes, nanowires, nanoribbons, and nanorods: Synthesis, characterizations, properties and applications. *Crit. Rev. Solid State Mater. Sci.* **37**, 1–74 (2012).
- Sahooli, M., Sabbaghi, S. & Saboori, R. Synthesis and characterization of mono sized CuO nanoparticles. *Mater. Lett.* **81**, 169–172 (2012).
- Dörner, L., Schmutz, P., Kägi, R., Kovalenko, M. V. & Jeurgens, L. P. H. Electrophoretic deposition of nanoporous oxide coatings from concentrated CuO nanoparticle dispersions. *Langmuir* **36**, 8075–8085 (2020).



28. Verma, N. & Kumar, N. Synthesis and biomedical applications of copper oxide nanoparticles: An expanding horizon. *ACS Biomater. Sci. Eng.* **5**, 1170–1188 (2019).
29. Tajima, K. *et al.* Mass-producible slit coating for large-area electrochromic devices. *Sol. Energy Mater. Sol. Cells* **232**, 111361 (2021).
30. Vetrivel, S., Saraswathi, M. S. S. A., Rana, D., Divya, K. & Nagendran, A. Cellulose acetate ultrafiltration membranes customized with copper oxide nanoparticles for efficient separation with antifouling behavior. *J. Appl. Polym. Sci.* **138**, 49867 (2021).
31. Kundu, M., Karunakaran, G., Kolesnikov, E., Gorshenkov, M. V. & Kuznetsov, D. Negative electrode comprised of nanostructured CuO for advanced lithium ion batteries. *J. Clust. Sci.* **28**, 1595–1604 (2017).
32. Buledi, J. A. *et al.* Heterogeneous kinetics of CuO nanoflakes in simultaneous decolourization of eosin Y and rhodamine b in aqueous media. *Appl. Nanosci.* **11**, 1241–1256 (2021).
33. Murinzi, T. W. *et al.* Copper oxide nanoparticles encapsulated in HKUST-1 metal-organic framework for electrocatalytic oxidation of citric acid. *J. Solid State Chem.* **268**, 198–206 (2018).
34. Omelyanchik, A. *et al.* Effect of citric acid on the morpho-structural and magnetic properties of ultrasmall iron oxide nanoparticles. *J. Alloys Compd.* **883**, 160779 (2021).
35. Abbas, A. *et al.* Silver nanoparticles modified electrodes for electroanalysis: An updated review and a perspective. *Microchem. J.* **175**, 107166 (2022).
36. Mahmood, A., Tezcan, F. & Kardaş, G. Photoelectrochemical characteristics of CuO films with different electrodeposition time. *Int. J. Hydrog. Energy* **42**, 23268–23275 (2017).
37. Dolai, S. *et al.* Cupric oxide (CuO) thin films prepared by reactive d.c. magnetron sputtering technique for photovoltaic application. *J. Alloys Compd.* **724**, 456–464 (2017).
38. Richardson, T. J., Slack, J. L. & Rubin, M. D. Electrochromism in copper oxide thin films. *Electrochim. Acta* **46**, 2281–2284 (2001).
39. Zeng, J. *et al.* Colourless-to-black electrochromic materials and solid-state devices with high optical contrast based on cross-linked poly(4-vinyltriphenylamine). *Sol. Energy Mater. Sol. Cells* **195**, 89–98 (2019).
40. Yu, X. *et al.* Colourless-to-black electrochromism from binary electrochromes toward multifunctional displays. *ACS Appl. Mater. Interfaces* **12**, 39505–39514 (2020).
41. Weng, D., Shi, Y., Zheng, J. & Xu, C. High performance black-to-transmissive electrochromic device with panchromatic absorption based on TiO<sub>2</sub>-supported viologen and triphenylamine derivatives. *Org. Electron.* **34**, 139–145 (2016).
42. Liu, H. S. *et al.* Highly transparent to truly black electrochromic devices based on an ambipolar system of polyamides and viologen. *NPG Asia Mater.* **9**, e388 (2017).
43. Greenwood, R. & Kendall, K. Selection of suitable dispersants for aqueous suspensions of zirconia and titania powders using acoustophoresis. *J. Eur. Ceram. Soc.* **19**, 479–488 (1999).
44. Hanaor, D., Michelazzi, M., Leonelli, C. & Sorrell, C. C. The effects of carboxylic acids on the aqueous dispersion and electrophoretic deposition of ZrO<sub>2</sub>. *J. Eur. Ceram. Soc.* **32**, 235–244 (2012).
45. Wu, C.-K., Yin, M., O'Brien, S. & Koberstein, J. T. Quantitative analysis of copper oxide nanoparticle composition and structure by X-ray photoelectron spectroscopy. *Chem. Mater.* **18**, 6054–6058 (2006).
46. Stadnichenko, A. I., Sorokin, A. M. & Boronin, A. I. XPS, UPS, and STM studies of nanostructured CuO films. *J. Struct. Chem.* **49**, 341–347 (2008).
47. Armelao, L. *et al.* A sol-gel approach to nanophase copper oxide thin films. *Thin Solid Films* **442**, 48–52 (2003).
48. Zhu, C., Oshero, A. & Panzer, M. J. Surface chemistry of electrodeposited Cu<sub>2</sub>O films studied by XPS. *Electrochim. Acta* **111**, 771–778 (2013).
49. Lindström, R. *et al.* Thin films of vanadium oxide grown on vanadium metal: oxidation conditions to produce V<sub>2</sub>O<sub>5</sub> films for Li-intercalation applications and characterization by XPS, AFM. *RBS/NRA. Surf. Interface Anal.* **38**, 6–18 (2006).
50. Dupin, J.-C., Gonbeau, D., Vinatier, P. & Levasseur, A. Systematic XPS studies of metal oxides, hydroxides and peroxides. *Phys. Chem. Chem. Phys.* **2**, 1319–1324 (2000).
51. Zhou, J.-H. *et al.* Characterization of surface oxygen complexes on carbon nanofibers by TPD, XPS and FT-IR. *Carbon* **45**, 785–796 (2007).
52. Rosenthal, D., Ruta, M., Schlögl, R. & Kiwi-Minsker, L. Combined XPS and TPD study of oxygen-functionalized carbon nanofibers grown on sintered metal fibers. *Carbon* **48**, 1835–1843 (2010).
53. Cheng, K.-C., Chen, F.-R. & Kai, J.-J. Electrochromic property of nano-composite Prussian Blue based thin film. *Electrochim. Acta* **52**, 3330–3335 (2007).
54. Neskovska, R., Ristova, M., Velevska, J. & Ristov, M. Electrochromism of the electroless deposited cuprous oxide films. *Thin Solid Films* **515**, 4717–4721 (2007).
55. Wang, C. *et al.* Controlled synthesis of micro/nanostructured CuO anodes for lithium-ion batteries. *Nano Energy* **9**, 334–344 (2014).
56. Arachi, Y. *et al.* Reversible electrochemical reaction of CuO with Li in the LiCuO<sub>2</sub> system. *Solid State Ion.* **225**, 611–614 (2012).
57. Morales, J. *et al.* Nanostructured CuO thin film electrodes prepared by spray pyrolysis: A simple method for enhancing the electrochemical performance of CuO in lithium cells. *Electrochim. Acta* **49**, 4589–4597 (2004).
58. Peng, J. *et al.* Experimental and theoretical investigation of the electronic structure of Cu<sub>2</sub>O and CuO thin films on Cu(110) using X-ray photoelectron and absorption spectroscopy. *J. Chem. Phys.* **138**, 024704 (2013).
59. Edström, K., Herstedt, M. & Abraham, D. P. A new look at the solid electrolyte interphase on graphite anodes in Li-ion batteries. *J. Power Sources* **153**, 380–384 (2006).
60. Jeong, C. Y. *et al.* Electrochromic properties of sputter-deposited rhodium oxide thin films of varying thickness. *Thin Solid Films* **709**, 138226-1–7 (2020).
61. Jeong, C. Y., Abe, Y., Kawamura, M., Kim, K. H. & Kiba, T. Electrochromic properties of rhodium oxide thin films prepared by reactive sputtering under an O<sub>2</sub> or H<sub>2</sub>O vapor atmosphere. *Sol. Energy Mater. Sol. Cells* **200**, 109976 (2019).
62. Yang, Y., Xu, D., Wu, Q. & Diao, P. Cu<sub>2</sub>O/CuO bilayered composite as a high-efficiency photocathode for photoelectrochemical hydrogen evolution reaction. *Sci. Rep.* **6**, 35158 (2016).
63. Huang, L., Peng, F. & Ohuchi, F. S. “In situ” XPS study of band structures at Cu<sub>2</sub>O/TiO<sub>2</sub> heterojunctions interface. *Surf. Sci.* **603**, 2825–2834 (2009).
64. Chang, Y., Teo, J. J. & Zeng, H. C. Formation of colloidal CuO nanocrystallites and their spherical aggregation and reductive transformation to hollow Cu<sub>2</sub>O nanospheres. *Langmuir* **21**, 1074–1079 (2005).
65. Oral, A. Y., Menşur, E., Aslan, M. H. & Başaran, E. The preparation of copper(II) oxide thin films and the study of their microstructures and optical properties. *Mater. Chem. Phys.* **83**, 140–144 (2004).
66. Ohya, Y., Ito, S., Ban, T. & Takahashi, Y. Preparation of CuO thin films and their electrical conductivity. *Key Eng. Mater.* **181–182**, 113–116 (2000).
67. Murali, D. S. *et al.* Synthesis of Cu<sub>2</sub>O from CuO thin films: Optical and electrical properties. *AIP Adv.* **5**, 047143 (2015).
68. Wu, J. T. & Liou, G. T. A novel panchromatic shutter based on an ambipolar electrochromic system without supporting electrolyte. *Chem. Commun.* **54**, 2619–2622 (2018).
69. Peng, B., Feng, C., Liu, S. & Zhang, R. Synthesis of CuO catalyst derived from HKUST-1 temple for the low-temperature NH<sub>3</sub>-SCR process. *Catal. Today* **314**, 122–128 (2018).
70. Nakate, U. T. *et al.* Nano-bitter gourd like structured CuO for enhanced hydrogen gas sensor application. *Int. J. Hydrog. Energy* **43**, 22705–22714 (2018).

71. Joshi, S., Mudigere, M., Krishnamurthy, L. & Shekar, G. Growth and morphological studies of NiO/CuO/ZnO based nanostructured thin films for photovoltaic applications. *Chem. Pap.* **68**, 1584–1592 (2014).
72. Zhou, Y. *et al.* Near-white light-emitting diode from p-CuO/n-GaN heterojunction with an i-CuO electron blocking layer. *J. Alloys Compd.* **867**, 159145 (2021).
73. Wang, Z. *et al.* Magnetolectric effect and phase transitions in CuO in external magnetic fields. *Nat. Commun.* **7**, 10295 (2016).
74. Fujita, K., Noda, T., Kojima, K. M., Eisaki, H. & Uchida, S. Effect of disorder outside the CuO<sub>2</sub> planes on T<sub>c</sub> of copper oxide superconductors. *Phys. Rev. Lett.* **95**, 097006 (2005).
75. Pourmortazavi, S. M., Kohsari, I. & Hajimirsadeghi, S. S. Electrosynthesis and thermal characterization of basic copper carbonate nanoparticles. *Cent. Eur. J. Chem.* **7**, 74–78 (2009).
76. Lee, K.-M. *et al.* Improvement of redox reactions by miniaturizing nanoparticles of zinc Prussian blue analog. *Appl. Phys. Lett.* **102**, 141901 (2013).
77. Lee, K.-M. *et al.* Accelerated coloration of electrochromic device with the counter electrode of nanoparticulate Prussian blue-type complexes. *Electrochim. Acta* **163**, 288–295 (2015).
78. Xiang, H. F., Xu, Z. X., Roy, V. A., Che, C. M. & Lai, P. T. Method for measurement of the density of thin films of small organic molecules. *Rev. Sci. Instrum.* **78**, 034104 (2007).

## Acknowledgements

This work was partially supported by JST A-STEP (Grant Number JPMJTR203D), Japan.

## Author contributions

C.Y.J.: Investigation, Writing-original draft, Writing-review & editing, Visualization. H.W.: Investigation, Writing-original draft, Writing-review & editing, Visualization. K.T.: Writing-original draft, Writing-review & editing, Supervision, Project administration.

## Competing interests

The authors declare no competing interests.

## Additional information

**Supplementary Information** The online version contains supplementary material available at <https://doi.org/10.1038/s41598-023-34839-9>.

**Correspondence** and requests for materials should be addressed to K.T.

**Reprints and permissions information** is available at [www.nature.com/reprints](http://www.nature.com/reprints).

**Publisher's note** Springer Nature remains neutral with regard to jurisdictional claims in published maps and institutional affiliations.



**Open Access** This article is licensed under a Creative Commons Attribution 4.0 International License, which permits use, sharing, adaptation, distribution and reproduction in any medium or format, as long as you give appropriate credit to the original author(s) and the source, provide a link to the Creative Commons licence, and indicate if changes were made. The images or other third party material in this article are included in the article's Creative Commons licence, unless indicated otherwise in a credit line to the material. If material is not included in the article's Creative Commons licence and your intended use is not permitted by statutory regulation or exceeds the permitted use, you will need to obtain permission directly from the copyright holder. To view a copy of this licence, visit <http://creativecommons.org/licenses/by/4.0/>.

© The Author(s) 2023